



HAL
open science

Oxygen diffusion and surface exchange coefficients measurements under high pressure: Comparative behavior of oxygen deficient versus over-stoichiometric air electrode materials

Jérôme Laurencin, Jacinthe Gamon, Aurélien Flura, Giuseppe Sdanghi, Sébastien Fourcade, Vibhu Vaibhav, Jean-Marc Bassat

► To cite this version:

Jérôme Laurencin, Jacinthe Gamon, Aurélien Flura, Giuseppe Sdanghi, Sébastien Fourcade, et al.. Oxygen diffusion and surface exchange coefficients measurements under high pressure: Comparative behavior of oxygen deficient versus over-stoichiometric air electrode materials. *Fuel Cells*, 2023, 23 (6), pp.366-376. <10.1002/fuce.202300048>. <hal-04200288>

HAL Id: hal-04200288

<https://hal.science/hal-04200288v1>

Submitted on 8 Sep 2023

HAL is a multi-disciplinary open access archive for the deposit and dissemination of scientific research documents, whether they are published or not. The documents may come from teaching and research institutions in France or abroad, or from public or private research centers.

L'archive ouverte pluridisciplinaire HAL, est destinée au dépôt et à la diffusion de documents scientifiques de niveau recherche, publiés ou non, émanant des établissements d'enseignement et de recherche français ou étrangers, des laboratoires publics ou privés.



Distributed under a Creative Commons CC BY-NC-ND 4.0 - Attribution - Non-commercial use - No Derivative Works - International License

Oxygen Diffusion and Surface Exchange Coefficients Measurements under High Pressure: Comparative Behaviour of Oxygen Deficient vs. Over-stoichiometric Air Electrode Materials

Jérôme Laurencin* (1), Jacinthe Gamon (2), Aurélien Flura (2), Giuseppe Sdanghi (1,2), Sébastien Fourcade (2), Vaibhav Vibhu (3), and Jean-Marc Bassat* (2)

(1) Univ. Grenoble Alpes – CEA/LITEN, 38054, Grenoble, France

(2) CNRS, Univ. Bordeaux, Bordeaux INP, ICMCB, 33600 Pessac, France

(3) Institute of Energy / Climate Research, IEK-9, FZJ GmbH, 52425 Jülich, Germany

*Corresponding authors: jerome.laurencin@cea.fr; jean-marc.bassat@icmcb.cnrs.fr

Abstract

Mixed ionic electronic conductors (MIECs) oxides are used as electrode materials for solid oxide cell (SOC) application, as they combine high electronic conductivity as well as high oxygen diffusivity and oxygen surface exchange coefficients. The ionic transport properties can be directly determined thanks to the isotopic exchange depth profiling (IEDP) method. To date, the reported measurements have been performed at ambient pressure and below. However, for a higher efficiency of hydrogen production at the system level, it is envisaged to operate the cell between 10 to 60 bar. To characterize the MIEC oxides properties in such conditions, an innovative setup able to operate up to a total pressure of 50 bar and 900 °C has been developed. The main goal of this study was to compare the behaviour of two types of reference materials: the oxygen deficient La-Sr-Fe-Co perovskites, and the overstoichiometric lanthanide nickelates $Ln_2NiO_{4+\delta}$ ($Ln = La, Pr, Nd$). Diffusion and surface exchange coefficients obtained under 6.3 bar of oxygen are measured and their evolution discussed in light of the change in oxygen stoichiometries. This analysis allows better understanding of the dependency of the surface exchange coefficient with the oxygen partial pressure.

Keywords

Oxygen Diffusion, Surface Exchange, MIEC Oxides, Oxygen Stoichiometry, Solid Oxide Cells

1. Introduction

Clean and sustainable energy sources are currently becoming essential. However, since the renewable energies are intermittent, efficient solutions for their storage are required, to match the fluctuations between the demand and the production. In this frame, hydrogen is considered as one of the most efficient energy vectors ^[1]. High temperature steam electrolysis (HTSE), based on the solid oxide electrolysis cells (SOEC) technology, is a promising and attractive solution for hydrogen production at high efficiency ^[2]. However, hydrogen has to be stored and distributed at high pressure. Therefore, since the compression of liquid water consumes much less energy than gaseous hydrogen, it is advantageous to perform the steam electrolysis directly under pressure ^[3]. Moreover, the high-temperature co-electrolysis of steam and carbon dioxide enables to convert electricity into a syngas composed of carbon monoxide and hydrogen ^[2,4]. This gas mixture can be transformed in a second step in liquid or gaseous hydrocarbons with conventional catalytic processes working at high pressure between 10 and 100 bar ^[5]. In this case, an integrated system working directly under pressure could also be beneficial in terms of efficiency and cost ^[3,6]. In this context, it is mandatory to investigate the impact of high pressure on the electro-catalytic properties of the electrode materials that control the cell electrochemical response, and more particularly the oxygen electrode, where the major polarization losses are observed.

Mixed ionic electronic conductors (MIECs) are commonly used as oxygen electrodes in SOEC cells. In addition to a high electronic conductivity, these materials exhibit both high oxygen diffusivity and surface exchange coefficient (D and k , respectively) at the operating temperatures. Two different kind of efficient candidates are generally considered: (i) the oxygen deficient perovskites such as $\text{La}_{0.6}\text{Sr}_{0.4}\text{CoO}_{3-\delta}$ (LSC) and $\text{La}_{0.6}\text{Sr}_{0.4}\text{Fe}_{0.8}\text{Co}_{0.2}\text{O}_{3-\delta}$ (LSFC) ^[7-11], which are nowadays the standard SOEC materials and (ii) the oxygen over-stoichiometric oxides, such as the lanthanide nickelates $\text{Ln}_2\text{NiO}_{4+\delta}$ ($\text{Ln} = \text{La}, \text{Pr}, \text{Nd}$), which belong to the so-called Ruddlesden-Popper series $\text{Ln}_{n+1}\text{Ni}_n\text{O}_{3n+1}$ (here with $n = 1$).^[12] These compounds show a K_2NiF_4 -type layered structure, with alternating LnNiO_3 perovskite layers and LnO rocksalt layers within which reside the additional interstitial oxygen atoms. The nickelates phases present promising oxygen electrode performances because of their large anionic bulk diffusion and surface exchange coefficients (approximately one order of magnitude higher than that of perovskites), combined with a good electrical conductivity and a thermal expansion coefficient matching with those of other cell components ^[13-15]. Railsback et al. showed that high pressure reduces the polarization resistance of oxygen electrodes for both over-stoichiometric and under-stoichiometric materials^[16]. They found that the improvement in performance with increasing pressure was more pronounced for the interstitial oxygen conducting materials. The difference in behaviour between the two types of material was related to the dependence of the oxygen defect concentration on $p\text{O}_2$.

Typically, D and k are measured *via* the electrical conductivity relaxation (ECR) method,^[17–20] or by the isotopic exchange depth profiling (IEDP) method.^[10,13,21–23] The latter technic involves to perform a ^{16}O for ^{18}O isotopic exchange on a crystal or dense pellet of the material at a desired temperature during an appropriate time. After the exchange, the depth profile of the ^{18}O tracer is determined *ex situ* using secondary mass ion spectroscopy (SIMS) technic. Using the Fick's second law, the tracer diffusion and surface exchange coefficients (here noted D^* and k^*) can be accessed by fitting the depth profiling data^[24]. To date, the reported measurements of D and k in literature have been performed at ambient pressure and below. To the best of our knowledge there is no available data for D and k measured at high pressure whatever the considered electrode material.

The objectives of this work consist in developing a $^{18}\text{O}/^{16}\text{O}$ exchange setup at high temperature able to work under high pressure of O_2 and assess the values of D^* and k^* in such conditions for various reference oxygen electrode materials: $\text{Ln}_2\text{NiO}_{4+\delta}$ ($\text{Ln} = \text{La}, \text{Pr}, \text{Nd}$), $\text{La}_{0.6}\text{Sr}_{0.4}\text{CoO}_{3-\delta}$ (LSC) and $\text{La}_{0.6}\text{Sr}_{0.4}\text{Fe}_{0.8}\text{Co}_{0.2}\text{O}_{3-\delta}$ (LSFC). The evolution of D^* and k with pressure will be discussed in light of the structural features and change in oxygen over-stoichiometry, δ , which is determined after the exchange.

2. Experimental

2.1. Powder Synthesis

Dense samples of the pure materials with a density of at least 95 % are required for the oxygen exchange experiments. In this study, pellets were prepared to fulfill these conditions, with a diameter of roughly 20 mm after sintering. Pure powders of the three lanthanide nickelates were produced using the modified Pechini method^[25] from Pr_6O_{11} (Aldrich chem, 99.9 %), La_2O_3 (99.99 %, Sigma Aldrich), Nd_2O_3 (Strem Chemical, 99.99 %) and $\text{Ni}(\text{NO}_3)_2 \cdot 6\text{H}_2\text{O}$ (Acros Organics, 99 %) precursors. La_2O_3 powder was initially heat-treated at 900 °C overnight to remove residual water before weighing. The final annealing was performed at 1,200 °C for 12 h in air, leading to well crystallized phases. $\text{La}_{0.58}\text{Sr}_{0.4}\text{Fe}_{0.8}\text{Co}_{0.2}\text{O}_{3-\delta}$ (LSFC) and $\text{La}_{0.58}\text{Sr}_{0.4}\text{CoO}_{3-\delta}$ (LSC) powders were synthesized by a standard solid-state route using the following precursors: La_2O_3 (99.99 %, Sigma Aldrich), SrCO_3 (99.9 %, Sigma Aldrich), Fe_2O_3 (99 %, Sigma Aldrich) and Co_3O_4 (99 %, Alfa Aeser). The powders were weighed according to the compositions and then ball-milled for 4 h at 250 rpm using zirconia balls and isopropanol (98.8 %, VWR). After drying at 80 °C overnight, the mixtures were then calcined in air at 1,080 °C for 8 h. The purity of all samples was controlled by X-ray diffraction (XRD) analysis before sintering.

2.2. Pellet Preparation

The powders were ball-milled for 4 h with isopropanol in order to get the average particle size $\sim 1 \mu\text{m}$. Dense pellets of the five materials were then produced by uniaxial pressing the powders in a 25 mm pellet die followed by a sintering at $1,350 \text{ }^\circ\text{C}$ for 4 h under air. The density of the pellet was measured geometrically and always exceeded 95 %.

For the five studied compositions, the dense pellets were first mirror polished, using abrasives of decreasing grain diameter, followed by diamond paste. Finally, cubes of roughly 4 mm side length were cut from the pellet, using a diamond cutting-disc (Isomet Buehler), to ensure comparable results from the sample.

2.3. Isotopic Exchange Under Pressure

2.3.1. Set-up Description

The isotopic oxygen exchange setup was developed for an operation under total pressure up to 40 bar and temperature up to $1,100 \text{ }^\circ\text{C}$ (Figure 1). It was more extensively described in ref. [26]. The first line of the setup is dedicated to high vacuum pumping: using a turbomolecular pump, a vacuum of roughly 10^{-6} mbar is obtained. The labelled ^{18}O gas (with isotopic purity close to 98 %) is routed through a second line, from a gas (air) cylinder provided by Euriso-top company with the following specifications: 1 L, $P = 20$ bar. Another line is dedicated to ^{16}O from the laboratory. A fourth line is dedicated to cryo-pumping of the labelled ^{18}O at the end of the exchange, which is achieved by immersing a stainless-steel rod (one meter long) into liquid helium. The gas may then be used for another experiment, provided that the ratio $^{18}\text{O}/^{16}\text{O}$ is still high. Two manometers allow measuring respectively the low and high pressures.

The sample holder is a closed cylinder made of magnesium doped zirconia, which was designed to withstand both the high pressure and high temperature in steady state operation as well as the stresses induced by quick thermal quenching. It was thus able to withstand, through all our experiments, rapid cooling from high operating temperature ($700 \text{ }^\circ\text{C} - 500 \text{ }^\circ\text{C}$) down to room temperature. This thermal quenching was achieved by removing the sample holder from the sliding furnace mounted on rails.

2.3.2. Procedure for the Isotopic Exchange Under Pressure

The experimental procedure for the IEDP method followed the procedure described in ref. [21]. In a first step, the samples were equilibrated at the target temperature ($700 \text{ }^\circ\text{C}$ for instance) in pure $^{16}\text{O}_2$ at a chosen pressure of 6.3 bar for a period at least ten times longer than the one chosen for the oxygen exchange experiment. The samples were then quenched down to room temperature. This first treatment creates the baseline in $^{18}\text{O}/^{16}\text{O}$ ratio inside the sample that will be used as reference for the subsequent time-of-flight secondary ion mass spectrometry (ToF-SIMS) analysis. Besides, it enables to equilibrate the oxygen (over or under)-stoichiometry at the given pressure and temperature

condition in the material. Next, the $^{16}\text{O}_2$ gas was pumped and replaced with the $^{18}\text{O}_2$ enriched (> 98 %) air mixture (specification described in section 2.3.1.) at room temperature. The total air pressure ($^{18}\text{O}_2/\text{N}_2$) injected into the reactor at room temperature was calculated to reach a total pressure of 30 bar at the studied temperature (following the ideal gas law: $P(300\text{ K}) = 30\text{ bar} \times 300\text{ K} / T_{\text{exchange}}$). Therefore, at the exchange temperature, the $^{18}\text{O}_2$ partial pressure is 6.3 bar (21 % \times 30 bar). The samples were quickly heated to reach the target temperature, and the oxygen exchange experiments carried out for a determined time. This time was calculated in order to obtain an approximate diffusion length L_D of a few tens of micrometers ($L_D \approx 2 \times \sqrt{D \times t}$) according to typical D values from the literature^[21]. Typically, the duration times used for the oxygen exchange steps varies from about 90 min at 700 °C till about 20 h at 500 °C. Samples were finally quenched down to room temperature, and $^{18}\text{O}_2$ recovered using liquid helium. Finally, the samples were taken out of the zirconia cylinder to be prepared for the ToF-SIMS analysis. Preliminary measurements, at $T = 600^\circ\text{C}$, were performed on the three studied nickelates, under 1 bar (air) of total pressure (instead of 30 bar in the main study). The results presented in Table S1 (cf. Supplementary Information, SI) show that the values obtained are in the same order of magnitude as the literature data. This validates the use of our setup for the measurement of D^* and k^* coefficients. Nevertheless, a difference of a factor of ~ 30 is obtained in the k^* coefficient for LNO, which could be attributed to a difference in grain orientation between the samples. Therefore, only large variation in the k^* coefficient will be discussed thereafter.

2.4. X-Ray Diffraction

Analysis of phase purity and lattice parameters were performed on a PANalytical X'Pert Pro diffractometer with a Cu source ($K\alpha_1$, $\lambda = 1.54060\text{ \AA}$) in reflection mode.

2.5. Thermogravimetric Analysis (TGA)

Our first goal was to determine the delta (δ) value characterizing the oxygen under/over-stoichiometric of the oxides, after each thermal treatment performed under pressure followed by a thermal quenching. For this purpose, thermogravimetric analysis (TGA) experiments were carried out using a TA Instrument[®] TGA-5500 device. First, the dense bar samples (after exchange experiments) were crushed into powder using mortar-pestle. Then the powders were heated under air up to $150\text{ }^\circ\text{C h}^{-1}$, then cooled down to room temperature with a slow rate ($2\text{ }^\circ\text{C min}^{-1}$), with the aim to remove any traces of water. A second cycle was performed under Ar - 5% H_2 flux with a very slow heating rate of ($0.5\text{ }^\circ\text{C min}^{-1}$) up to $1,000\text{ }^\circ\text{C}$. The full decomposition of the material under reducing atmosphere leads to the determination of the oxygen stoichiometry after cycling the sample down to room temperature. The decomposition products (Ln_2O_3 , SrO, metallic Ni, Fe and Co) were verified by XRD after the thermal cycle. However, despite several attempts, the complete reduction of LSFC

under Ar – 5 % H₂ flux was never reached (the XRD analyses evidenced the formation of (La,Sr)₂(Fe,Co)O₄ + Fe + Co) inhibiting the calculation of δ in this case.

2.6. Time-of-Flight Secondary Ion Mass Spectrometry (ToF-SIMS) Analysis

2.6.1. Preparation

Prior to the ToF-SIMS analysis, the cubes were cut in half with the utmost care using the diamond cutting-disc. This cut is necessary to reveal the gradient in ¹⁸O. The new face created was then mirror polished. The resulting two samples were fixed inside a stainless-steel ring with Wood's metal alloy in such a way that one of the samples exposes the bulk of the cube that contains the gradient of ¹⁸O, while the other exposes the surface of the cube that was in direct contact with ¹⁸O₂. The latter preparation enables to measure with precision the ratio ¹⁸O/¹⁶O at the surface of the sample, averaged over a large area. This value is used as the origin of the gradient measured on the “depth profile” sample.

2.6.2. SIMS

SIMS experiments were performed using a ToF SIMS 5 (IONTOF, Münster, Germany). Samples were analysed in spectroscopy mode by scanning a primary 30 keV Bi⁺ beam over 500 × 500 μm² area, interlaced with a 1 keV Cs⁺ sputter beam scanned over 600 × 600 μm² to eliminate surface impurities and enhance production of negative secondary ions. The region of interest (ROI) was adjusted using the integrated optical camera and sample stage controls. The ROI was chosen so that a sample edge was located vertically on the right or left of the raster field of view. Data acquisition was started in the 3D mode, and the following procedure was used to determine the stopping condition: once the secondary ions of interest (e.g. ¹⁸O and ¹⁶O) peaks were selected on the spectra subpanel, images of ion intensity with definition 256 × 256 pixels were automatically generated by the instrument software (SurfaceLab 7) in the image stockpile subpanel. The images of ¹⁸O and ¹⁶O intensities were then combined to generate an image of the isotopic ratio of interest $I(^{18}\text{O})/(I(^{18}\text{O})+I(^{16}\text{O}))$. An average line scan was then performed using the X-area feature of SurfaceLab linescan editor. This procedure enabled us to follow the gradient line-scan progress in real-time so that data acquisition could be stopped, typically after 5 to 10 min, when the gradient was stabilized at a good signal to noise ratio. Doing so an isotopic ratio profile averaged over a volume of approx. 500 × 500 × 0.1 μm³ was generated, which allows minimizing artifacts from impurities and inhomogeneities. The data were finally exported as ASCII file for further analysis (Figure S2 and S3). In some cases, ¹⁸O gradient spanned over 500 μm so that a second adjacent area was analysed similarly and stitched to the previous one.

The experimental oxygen profiles (evolution of $I(^{18}\text{O})/I(^{18}\text{O})+I(^{16}\text{O})$ vs. depth) were then fitted using the Crank solution to the equation of the second Fick's law of gas diffusion in solids ^[21,27], which leads determining the D^* and k^* coefficients (* being relative to the diffusion of the ^{18}O tracer).

3. Results and Discussion

3.1. Oxygen Stoichiometry

After the oxygen exchange under pressure steps, the samples were quenched to stop the oxygen diffusion as to keep the same oxygen composition that was reached in the material during the investigated experimental conditions: $p\text{O}_2 = 6.3$ bar (total pressure (air) around 30 bar), $500 < T / ^\circ\text{C} < 700$. Purity of the sample after the exchange was checked with XRD, showing the phases are stable in the high O_2 pressure conditions at the investigated temperatures. Moreover, the ToF-SIMS images reveal that the surface is smooth with no visible cracks (Figure S1). Our first goal was to determine the corresponding oxygen stoichiometry values of the materials exposed to the O_2 high pressure. For this purpose, we used TGA experiments performed under reducing atmosphere (Ar- 5 % H_2 flow) on powders (crushed pellets). Regarding the nickelate phases with oxygen overstoichiometry, the decomposition of the oxide occurs in two steps: (i) at intermediate temperature a first plateau is evidenced, which corresponds to the stabilization of the oxide only containing Ni^{II} , i.e. a composition $\text{Ln}_2\text{NiO}_{4.0}$ ($\text{Ln} = \text{La}, \text{Pr}, \text{Nd}$). The measured weight loss between room temperature and this plateau temperature corresponds exactly to the disappearance of the oxygen overstoichiometry δ . (ii) In a second step, at higher temperature, the full decomposition of the oxide is observed, leading, as checked by XRD, to the formation of Ln_2O_3 plus metallic nickel. The measure of the weight loss recorded between room temperature and the full reduction is then another way to determine δ . Regarding LSC, the full reduction is observed on the TGA curves, with no intermediate reduction plateau. As stated in the Experimental Section, the value of δ could not be determined for LSCF as the full reduction of the material could not be achieved. Table 1 gathers the oxygen stoichiometry results obtained for each exchanged sample, for $500 < T / ^\circ\text{C} < 700$ and $p\text{O}_2 = 6.3$ bar (total pressure around 30 bar). For the nickelates, each reported δ value is an average of the two calculations detailed above.

As expected, whatever the temperature used for the oxygen exchange, all materials exhibit a significant increase of the oxygen stoichiometry after the thermal treatment performed under high oxygen pressure, compared to the value obtained after the chemical synthesis. Indeed, the compositions determined at room temperature after the synthesis performed in air were: $\text{La}_2\text{NiO}_{4.16(2)}$, $\text{Pr}_2\text{NiO}_{4.22(2)}$, $\text{Nd}_2\text{NiO}_{4.21(3)}$ and $\text{La}_{0.58}\text{Sr}_{0.4}\text{CoO}_{2.980(14)}$, compared to $\text{La}_2\text{NiO}_{4.23(2)}$, $\text{Pr}_2\text{NiO}_{4.50(2)}$, $\text{Nd}_2\text{NiO}_{4.28(3)}$ and $\text{La}_{0.58}\text{Sr}_{0.4}\text{CoO}_{2.997(14)}$ (for $T_{\text{ex}} = 700$ °C) revealing that the studied compositions are

significantly more oxidized after the thermal treatments performed under ^{18}O pressure, with respect to ambient pressure. Considering the error bar, the LSC compound is found to be fully stoichiometric: $\text{La}_{0.58}\text{Sr}_{0.4}\text{CoO}_3$. This result is in good agreement with the calculation from Railsback et al., where oxygen defect concentrations were derived from electrochemical impedance spectra measured at high pressure.^[16] Interestingly, for $\text{Pr}_2\text{NiO}_{4+\delta}$, the oxygen overstoichiometry is considerably higher than that obtained for $\text{La}_2\text{NiO}_{4+\delta}$ and $\text{Nd}_2\text{NiO}_{4+\delta}$. Although it is commonly accepted for $\text{Pr}_2\text{NiO}_{4+\delta}$ and $\text{Nd}_2\text{NiO}_{4+\delta}$ to accept larger extent of oxygen overstoichiometry compared to $\text{La}_2\text{NiO}_{4+\delta}$ due to the smaller size of the lanthanide ions, here $\text{Nd}_2\text{NiO}_{4+\delta}$ does not show such high δ value. Moreover, this trend is repeatable over the whole temperature range studied with δ always exceeding 0.3 and reaching a maximum of 0.5 for an exchange at 700 °C. It was formally considered that Pr^{4+} could be present in the $\text{Pr}_2\text{NiO}_{4+\delta}$ compound, but XANES studies concluded in the absence of this species in the compound prepared under ambient atmosphere pressure^[28]. Here, the high pressure of oxygen could be a driving force for the stabilization of Pr^{4+} , which could be an explanation for the large oxygen overstoichiometries. This hypothesis will need to be confirmed by further studies. It is the first time that such remarkably high δ values have been observed in these compounds. This property is expected to have a high impact on the electrochemical performances by promoting the bulk path in the electrode ^[29].

3.2. Diffusion

Figures 2 and 3 show the evolution of the D^* coefficients as a function of $1000/T$ for the over-oxidized nickelates and for the oxide deficient perovskites, respectively, obtained from the fit of the ^{18}O gradients (Figure S2 and S3).

As it could be expected, the D^* coefficient for both types of materials shows a different evolution with increasing of oxygen pressure from $p\text{O}_2 = 0.2$ bar to 6.3 bar. For $\text{La}_2\text{NiO}_{4+\delta}$ and $\text{Pr}_2\text{NiO}_{4+\delta}$, D^* is slightly enhanced over the whole temperature range when the pressure is increased. For $\text{Nd}_2\text{NiO}_{4+\delta}$, the improvement is only observed for a temperature higher than 650 °C (Figure 2). However, D^* decreases by approximately one order of magnitude for the oxide deficient perovskites over the whole studied temperature range (Figure 3).

Some years ago Chronos et al.^[30], and Parfitt et al.^[31] have performed molecular dynamics (MD) simulations regarding the oxygen diffusion in $\text{La}_2\text{NiO}_{4+\delta}$ and $\text{Pr}_2\text{NiO}_{4+\delta}$, respectively. The dominant mechanism of oxygen transport occurs *via* the network of apical oxygen sites connected by interstitial ion sites along a two-dimensional network (the so-called interstitialcy mechanism^[30]). In the article by Parfitt et al., the oxygen diffusivities were calculated for a range of hyper-stoichiometries, and an excellent agreement was found between the absolute calculated values and those observed

experimentally. From $\delta = 0$, the diffusivity rises very quickly as a function of δ , but rapidly levels off. Between $\delta = 0.05$ and $\delta = 0.25$ the diffusivity still increases but more smoothly. This can be explained by the increase of the formation energy of oxygen interstitials at high δ values, as well as the stiffening of the lattice caused by the additional oxygen interstitial pinning the NiO_6 sub-lattice, which reduces the passage of the oxygen ions. Our results are in good agreement with such calculations. Indeed when increasing δ for each studied nickelate through high oxygen pressure, a limited increase of the diffusion coefficient is observed, although a larger one could be expected in a first approximation. The largest increase is observed for $\text{La}_2\text{NiO}_{4+\delta}$, for which the initial oxygen overstoichiometry is the lowest compared to $\text{Pr}_2\text{NiO}_{4+\delta}$ and $\text{Nd}_2\text{NiO}_{4+\delta}$ ($\delta = 0.16$ at room temperature after annealing under air at normal pressure, cf. Table 1).

Considering these results, and in accordance with data obtained at $p\text{O}_2 < 1$ atm from the literature (cf. Figure S4),^[32] one would expect the activation energies for D^* to increase from 0.2 bar to 6.3 bar. An overall increase in the activation energy was measured for $\text{Nd}_2\text{NiO}_{4+\delta}$ by Yakal-Kremiski et al. in a lower $p\text{O}_2$ range.^[32] Although this evolution is observed for $\text{Nd}_2\text{NiO}_{4+\delta}$ and $\text{Pr}_2\text{NiO}_{4+\delta}$ (105 and 75 kJ mol^{-1} at 0.2 bar compared to 174 and 84 kJ mol^{-1} at 6.3 bar for $\text{Nd}_2\text{NiO}_{4+\delta}$ and $\text{Pr}_2\text{NiO}_{4+\delta}$, respectively), on the contrary for $\text{La}_2\text{NiO}_{4+\delta}$, the activation energy decreases with increasing pressure: from 97 kJ mol^{-1} at 0.2 bar to 55 kJ mol^{-1} at 6.3 bar. This could be attributed to the smaller value of δ which limits the effect of lattice stiffening. These assumptions remain to be further studied through combined experimental and theoretical studies.

In the oxide deficient perovskite material, the oxygen diffusion coefficient, D_O , is linked to the concentration of oxide vacancies, c_v , through the relationship:

$$D_O = D_v c_v / c_O \quad \text{Eq. (1)}$$

Where D_v is the vacancy diffusion coefficient and c_O the concentration of oxygen in the perovskite.^[33] It was formerly demonstrated that the tracer diffusion coefficient of oxide ions in perovskite materials is proportional to the oxide ion vacancy concentration.^[23]

Therefore, the decrease in D^* with pressure is directly explained by the decrease of δ at high oxygen pressure. Moreover, activation energies at 6.3 bar (179 and 223 $\text{kJ}\cdot\text{mol}^{-1}$ for LSC and LSCF, respectively) are similar to those obtained at 0.2 bar (175 and 191 $\text{kJ}\cdot\text{mol}^{-1}$ for LSC and LSCF, respectively). For this high $p\text{O}_2$, the compounds appear to be close to the stoichiometry in such a way that there is not a large variation of c_v with temperature (cf. Table 1). Therefore, we can expect a similar activation energy for D_v and D_O . The fact that these two parameters do not exhibit a strong variation suggests that neither structural change nor difference in diffusion mechanism occurs with increased pressure.

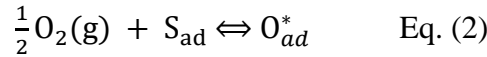
3.3. Surface Exchange

The evolution of the k^* coefficients vs. $1000/T$ is plotted on Figures 4 and 5 for the over-oxidized nickelates and for the oxide deficient perovskites, respectively.

For the three considered nickelate samples, the k^* coefficients are improved after oxygen exchanges performed under pressure compared to the corresponding values obtained after oxygen exchange performed under $pO_2 = 0.2$ bar. On the contrary, for both oxygen deficient perovskite materials, the surface exchange coefficient does not show a strong change with increasing from $pO_2 = 0.2$ bar to $pO_2 = 6.3$ bar (Figure 5).

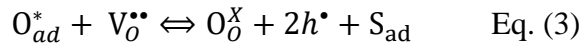
Surface exchange in oxygen deficient perovskite oxide materials has been studied for a long time in literature [22,34–36]. The oxygen incorporation mechanism can be described by two successive steps:

(i) step 1, dissociative adsorption:

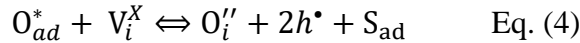


And (ii) step 2, incorporation:

For oxide deficient materials:



For overstoichiometric oxide materials:



Where S_{ad} is an adsorption site, $V_O^{\bullet\bullet}$ an oxide vacancy, V_i^X a vacant interstitial site and h^\bullet an electronic hole.

The corresponding thermodynamic equilibrium constants are given by:

$$K_{ads} = \frac{[O_{ad}^*]}{pO_2^{1/2} \times [S_{ad}]} \quad \text{Eq. (5)}$$

$$K_{inc} = \frac{[O_O^X][S_{ad}][h^\bullet]^2}{[O_{ad}^*][V_O^{\bullet\bullet}]} \quad \text{Eq. (6)}$$

$$K'_{inc} = \frac{[O_O^X][S_{ad}][h^\bullet]^2}{[O_{ad}^*][V_i^X]} \quad \text{Eq. (7)}$$

Here, $[O_O^X]$, $[S_{ad}]$, and $[h^\bullet]$ can be considered as constants, with the hypotheses that (i) the under- or over-stoichiometry remains low compared to the oxygen in the material, (ii) the coverage rate is low compared to the amount of adsorption sites and (iii) a high electronic conductivity. The surface exchange coefficient, $k^* / \text{cm s}^{-1}$ is proportional to the surface exchange kinetic rate, $v / \text{mol O m}^2 \text{ s}^{-1}$ through the relationship: $k^* = v/c_O$.^[37] Therefore, the evolution of k^* with pO_2 follows that of the

kinetic rate, which will be discussed hereafter. Considering a first order reaction kinetic, the corresponding rates to Eq. (5), (6) and (7) can be written as:

$$v_{ads} = k_{f,ads}(pO_2)^{\frac{1}{2}}[S_{ad}] - k_{b,ads}[O_{ad}^*] \quad \text{Eq. (8)}$$

$$v_{inc} = k_{f,inc}[O_{ad}^*][V_O^{\bullet\bullet}] - k_{b,inc} \quad \text{Eq. (9)}$$

$$v'_{inc} = k_{f,inc}[O_{ad}^*][V_i^X] - k_{b,inc} \quad \text{Eq. (10)}$$

where k_f and k_b denote the forward and backward kinetic constants of the reaction, respectively.

As has been shown by van Doorn et al. [35], through Eq. (5), it can be seen that $[O_{ad}^*]$ varies as the square root of pO_2 . Therefore, if the adsorption step is the rate determining step (r.d.s), the kinetic rate of the reaction should vary as the square root of oxygen partial pressure.

Bouwmeester et al. showed that dissociative adsorption is a rate-determining step in $La_2NiO_{4+\delta}$ and $Pr_2NiO_{4+\delta}$, whereas, for instance in perovskite $PrNiO_{3-\delta}$, both mechanisms are in competition, with the incorporation becoming the rate limiting step from 550 °C [38]. Thereby, the observed increase in the surface exchange coefficient k^* in the layered nickelates is consistent with the theoretical dependence of the r.d.s adsorption kinetic rate with $pO_2^{1/2}$. Along with the slight increase of the diffusion coefficient, this result reinforces the attractiveness of the lanthanide nickelate materials as innovative oxygen electrodes for the SOEC application under pressure.

Interestingly, the activation energy for the surface exchange process shows a strong increase for $Pr_2NiO_{4+\delta}$ and $Nd_2NiO_{4+\delta}$ with increasing pO_2 : from 45 kJ mol⁻¹ and 41 kJ mol⁻¹ at $pO_2 = 0.2$ bar [13] to 102 kJ mol⁻¹ and 104 kJ mol⁻¹ at $pO_2 = 6.3$ bar for $Pr_2NiO_{4+\delta}$ and $Nd_2NiO_{4+\delta}$, respectively. On the opposite, this increase is very limited for $La_2NiO_{4+\delta}$, with activation energies of 50 kJ mol⁻¹ at $pO_2 = 0.2$ bar [13] and 54 kJ mol⁻¹ at $pO_2 = 6.3$ bar. Staykov et al. studied the electrochemical activity of $La_2NiO_{4+\delta}$ and $Pr_2NiO_{4+\delta}$ through density functional theory (DFT) simulations. [39] Their results show that as interstitial oxygen atoms are accommodated in the rocksalt layer, the activation energy for O_2 dissociation is increased due to an increase in the material work function. Indeed, the electronic holes created in the Ln valence bands reduce the ability of the material to donate electrons. [39] This could explain why, for $Pr_2NiO_{4+\delta}$ and $Nd_2NiO_{4+\delta}$, which show particularly strong oxygen over-stoichiometry at high pressure, the activation energy for surface exchange increases, on the contrary to $La_2NiO_{4+\delta}$ for which δ is maintained below 0.25.

In comparison, the fact that k^* does not increase with pO_2 in LSC and LSCF rather suggests that the incorporation step is rate determining in those materials, as already suggested by previous studies from the literature for $La_{1-x}Sr_xCoO_{3-\delta}$ ($x = [0.1-0.9]$) [35,40]. It is also consistent with the result obtained by Bouwmeester et al. on another oxide deficient material, i.e. $PrNiO_{3-\delta}$ [38]. According to equation (6), if the incorporation rate is the rate limiting step, the pO_2 dependence of the surface

exchange rate also depends on the variation of the oxide vacancy or interstitial concentration, because this one also varies as a function of pO_2 . The dependence of δ ($\delta = [V_O^{\bullet\bullet}]$) with pO_2 has been studied in $La_{1-x}Sr_xCoO_{3-\delta}$ ($x = [0.1-0.9]$)^[41] and $La_{0.6}Sr_{0.4}Fe_{0.2}Co_{0.8}O_{3-\delta}$ ^[34] for $pO_2 \leq 1$ bar. In $La_{1-x}Sr_xCoO_{3-\delta}$, for low δ values (i.e. at low temperatures and for low x values), δ varies strongly with pO_2 , and is almost proportional to $pO_2^{-0.5}$ ^[41], thereby canceling out the pO_2 dependence of v_{inc} with pO_2 . This would explain why, for low δ values, k^* is almost independent of pO_2 . As the concentration of oxide vacancies increase in the material, the pO_2 dependence decreases (e.g. $\delta \propto pO_2^{-0.21}$ for $La_{0.7}Sr_{0.3}CoO_{3-\delta}$ at 500 °C and $\delta \propto pO_2^{-0.07}$ for $La_{0.3}Sr_{0.7}CoO_{3-\delta}$ at 800 °C), and k^* increases as pO_2 increases. Interestingly, for both materials, we note that the $\log \delta$ vs. $\log pO_2$ is only linear over a limited pO_2 range, and the slope increases in the high pO_2 region^[34,41]. This trend is highlighted in Figure 6, where our data for $La_{0.58}Sr_{0.4}CoO_{3-\delta}$ are compared with those of the literature.

We suspect that in our materials, which exhibit low oxide vacancy concentration, at such high oxygen partial pressure, the pO_2 dependence of δ is strong (possibly close to -0.5, as seen on Figure 6 for LSC), which explains why k^* does not vary strongly with pO_2 . The high pressure condition studied in this work should thus explain why the results obtained on k^* stand in contrast with previous report from the literature which showed that the surface exchange coefficient increases with increasing pO_2 , for $pO_2 < 1$ bar. Moreover, the pO_2 dependence of surface exchange is expected to behave differently under operating conditions, since the electrode polarization modifies the concentration profile of oxygen vacancies at the surface.^[42,43] Overall, these results confirm that there exists a fundamental limit to k^* for oxygen deficient perovskites, as observed by De Souza et al.^[22,42,44]

4. Conclusions

To increase the efficiency of solid oxide electrolyzers at the system level, it is envisaged to operate at high pressure. In this context, the goal of this work was to determine the oxygen diffusion and surface exchange coefficients of two standard under-stoichiometric oxygen electrode materials: $La_{0.6}Sr_{0.4}CoO_{3-\delta}$ and $La_{0.6}Sr_{0.4}Fe_{0.8}Co_{0.2}O_{3-\delta}$ and three over-stoichiometric nickelates: $La_2NiO_{4+\delta}$, $Pr_2NiO_{4+\delta}$ and $Nd_2NiO_{4+\delta}$. These latter materials have been developed for several years as alternative oxygen electrodes to the more conventional oxygen deficient perovskites. The measurements were performed using the IEDP method. For this purpose, an original set-up able to operate up to a total pressure of 50 bar and 900 °C has been developed.

As expected, the five materials became over oxidized after the oxygen isotopic exchanges performed in the temperature range $500 < T / ^\circ C < 700$ under $pO_2 \sim 6.3$ bar compared to the as-prepared ones (under atmospheric condition at $pO_2 \sim 0.2$ bar). The measured evolutions of D^* and k^* coefficients are thus representative of materials in a very different oxidation state. For LSC and LSFC, the thermal treatments performed under pressure induces a large decrease of the concentration of oxide vacancies

and both the D^* and k^* coefficients values are significantly lowered when increasing the pressure up to 6.3 bar. On the contrary, the oxygen over-stoichiometry of the nickelates is enlarged after the thermal treatment under pressure, and D^* and k^* coefficients are found to increase compared to ambient pressure measurements at sufficiently high temperature. The increase is particularly marked for k^* coefficient with up to around one order of magnitude increase is found for $\text{Pr}_2\text{NiO}_{4+\delta}$. The different evolution of the k^* coefficient with increased pressure could be explained by the difference in the rate limiting step of the oxygen exchange reaction. For lanthanide nickelates, it is governed by dissociative adsorption (proportional to $p\text{O}_2^{0.5}$), whereas in the perovskites, incorporation is the rate determining, with the kinetics depending on the oxide vacancy concentration. The results obtained in this work contrast with that of previous report from the literature, which can be explain by the difference in the pressure condition used. This study therefore paves the way for further screening of MIEC material properties at $p\text{O}_2 > 1$ bar, which will contribute to the thorough understanding of their exchange and diffusion mechanistic behaviors.

Moreover, these results strongly support that the electrochemical performances of the lanthanide nickelates with MIEC properties should improve during SOEC operation under pressure. This further reinforces their attractiveness compared to the cobalt based perovskites for which the amount of oxygen vacancy becomes too low in the same operating conditions, limiting the ionic transport properties of the corresponding electrodes. Nevertheless, the long-term stability of these materials when submitted to high pressure and polarization still needs to be studied.

Acknowledgments

A.F. thanks the CNRS French grouping GDR HysPàc for supporting this research work *via* an internal project. CEA is acknowledged for its valuable technical aid, including the supply of the pressurized air bottle enriched in ^{18}O . The authors strongly acknowledge Pr. John Kilner (Imperial College London) for fruitful discussions. We thank Jean-Paul Salvétat and the « PLateforme Aquitaine de CARactérisation des MATériaux », PLACAMAT: UAR 3626 for performing the ToF-SIMS experiment and for valuable discussions.

List of Symbols

c_v	Concentration of oxide vacancies / cm^{-3}
c_{O}	Concentration of oxygen in the perovskite / cm^{-3}
D	Oxygen diffusion coefficient / $\text{cm}^2 \text{s}^{-1}$
D_{O}	Oxygen diffusion coefficient / $\text{cm}^2 \text{s}^{-1}$
D_v	Vacancy diffusion coefficient / $\text{cm}^2 \text{s}^{-1}$
D^*	Oxygen tracer diffusion coefficient / $\text{cm}^2 \text{s}^{-1}$
δ	Oxygen over or under stoichiometry
h^\bullet	Electronic hole
K	Thermodynamic equilibrium constants
k	Oxygen surface exchange coefficient / cm s^{-1}
k^*	Oxygen tracer surface exchange coefficient / cm s^{-1}
k_b	Backward kinetic constant
k_f	Forward kinetic constant
p_{O_2}	Oxygen partial pressure / bar
S_{ad}	Adsorption site
T_{ex}	Temperature of the exchange / $^\circ\text{C}$
v	Surface exchange kinetic rate / $\text{mol m}^{-2} \text{s}^{-1}$
$V_{\text{O}}^{\bullet\bullet}$	Oxide vacancy
V_i^X	Vacant interstitial site

References

- [1] T. N. Veziroğlu, F. Barbir, *International Journal of Hydrogen Energy* **1992**, *17*, 527.
- [2] S. D. Ebbesen, S. H. Jensen, A. Hauch, M. B. Mogensen, *Chem. Rev.* **2014**, *114*, 10697.
- [3] E. Giglio, A. Lanzini, M. Santarelli, P. Leone, *Journal of Energy Storage* **2015**, *2*, 64.
- [4] Y. Wang, T. Liu, L. Lei, F. Chen, *Fuel Processing Technology* **2017**, *161*, 248.
- [5] W. Keim, Ed., *Catalysis in CI Chemistry*, Vol. 4, Springer Netherlands, Dordrecht, **1983**.
- [6] J. B. Hansen, N. Christiansen, J. U. Nielsen, *ECS Trans.* **2011**, *35*, 2941.
- [7] M. A. Laguna-Bercero, *Journal of Power Sources* **2012**, *203*, 4.
- [8] A. Hauch, R. Küngas, P. Blennow, A. B. Hansen, J. B. Hansen, B. V. Mathiesen, M. B. Mogensen, *Science* **2020**, *370*, eaba6118.
- [9] M. Y. Lu, J. G. Railsback, H. Wang, Q. Liu, Y. A. Chart, S.-L. Zhang, S. A. Barnett, *J. Mater. Chem. A* **2019**, *7*, 13531.
- [10] A. V. Berenov, A. Atkinson, J. A. Kilner, E. Bucher, W. Sitte, *Solid State Ionics* **2010**, *181*, 819.
- [11] S. J. Benson, PhD Thesis, Department of Materials, Imperial College, London, **1999**.
- [12] M. A. Morales-Zapata, A. Larrea, M. A. Laguna-Bercero, *Electrochimica Acta* **2023**, *444*, 141970.
- [13] E. Boehm, J. Bassat, P. Dordor, F. Mauvy, J. Grenier, P. Stevens, *Solid State Ionics* **2005**, *176*, 2717.
- [14] A. Aguadero, J. A. Alonso, M. J. Martinez-Lope, M. T. Fernandez-Diaz, M. J. Escudero, L. Daza, *J. Mater. Chem.* **2006**, *16*, 3402.
- [15] A. Flura, S. Dru, C. Nicollet, V. Vibhu, S. Fourcade, E. Lebraud, A. Rougier, J.-M. Bassat, J.-C. Grenier, *Journal of Solid State Chemistry* **2015**, *228*, 189.
- [16] J. Railsback, G. Hughes, L. Mogni, A. Montenegro-Hernández, S. Barnett, *J. Electrochem. Soc.* **2016**, *163*, F1433.
- [17] S. Wang, P. A. W. van der Heide, C. Chavez, A. J. Jacobson, S. B. Adler, *Solid State Ionics* **2003**, *156*, 201.
- [18] M. Yang, E. Bucher, W. Sitte, *Journal of Power Sources* **2011**, *196*, 7313.
- [19] A. Egger, E. Bucher, M. Yang, W. Sitte, *Solid State Ionics* **2012**, *225*, 55.
- [20] J. E. ten Elshof, M. H. R. Lankhorst, H. J. M. Bouwmeester, *Solid State Ionics* **1997**, *99*, 15.
- [21] J.-M. Bassat, M. Petitjean, J. Fouletier, C. Lalanne, G. Caboche, F. Mauvy, J.-C. Grenier, *Applied Catalysis A: General* **2005**, *289*, 84.
- [22] R. A. De Souza, J. A. Kilner, *Solid State Ionics* **1999**, *126*, 153.

- [23] T. Ishigaki, S. Yamauchi, K. Kishio, J. Mizusaki, K. Fueki, *Journal of Solid State Chemistry* **1988**, *73*, 179.
- [24] J. A. Kilner, S. J. Skinner, H. H. Brongersma, *Journal of Solid State Electrochemistry* **2011**, *15*, 861.
- [25] Ph. Courty, H. Ajot, Ch. Marcilly, B. Delmon, *Powder Technology* **1973**, *7*, 21.
- [26] A. Flura, J. Laurencin, S. Fourcade, F. Mauvy, V. Vibhu, J.-P. Salvetat, J. Mouginn, J.-M. Bassat, *ECS Trans.* **2021**, *103*, 1319.
- [27] J. Crank, *The Mathematics of Diffusion*, Clarendon Press, **1975**.
- [28] T. Ogier, C. Prestipino, S. Figueroa, F. Mauvy, J. Mouginn, J. C. Grenier, A. Demourgues, J. M. Bassat, *Chemical Physics Letters* **2019**, *727*, 116.
- [29] G. Sdanghi, L. Yefsah, F. Mauvy, E. Djurado, T. David, J.-M. Bassat, J. Laurencin, *J. Electrochem. Soc.* **2022**, *169*, 034518.
- [30] A. Chroneos, D. Parfitt, J. A. Kilner, R. W. Grimes, *J. Mater. Chem.* **2010**, *20*, 266.
- [31] D. Parfitt, A. Chroneos, J. A. Kilner, R. W. Grimes, *Physical Chemistry Chemical Physics* **2010**, *12*, 6834.
- [32] K. Yakal-Kremiski, L. V. Moggi, A. Montenegro-Hernández, A. Caneiro, S. A. Barnett, *J. Electrochem. Soc.* **2014**, *161*, F1366.
- [33] R. A. De Souza, J. A. Kilner, *Solid State Ionics* **1998**, *106*, 175.
- [34] M. Katsuki, S. Wang, M. Dokiya, T. Hashimoto, *Solid State Ionics* **2003**, *156*, 453.
- [35] R. H. E. van Doorn, I. C. Fullarton, R. A. de Souza, J. A. Kilner, H. J. M. Bouwmeester, A. J. Burggraaf, *Solid State Ionics* **1997**, *96*, 1.
- [36] B. A. Boukamp, B. A. van Hassel, I. C. Vinke, K. J. De Vries, A. J. Burggraaf, *Electrochimica Acta* **1993**, *38*, 1817.
- [37] H. J. M. Bouwmeester, C. Song, J. Zhu, J. Yi, M. van Sint Annaland, B. A. Boukamp, *Phys. Chem. Chem. Phys.* **2009**, *11*, 9640.
- [38] S. Saher, J. Song, V. Vibhu, C. Nicollet, A. Flura, J.-M. Bassat, H. J. M. Bouwmeester, *J. Mater. Chem. A* **2018**, *6*, 8331.
- [39] A. Staykov, T. Nguyen, T. Akbay, T. Ishihara, *The Journal of Physical Chemistry C* **2022**, *126*, 7390.
- [40] Y. Takeda, R. Kanno, M. Noda, Y. Tomida, O. Yamamoto, *J. Electrochem. Soc.* **1987**, *134*, 2656.
- [41] J. Mizusaki, Y. Mima, S. Yamauchi, K. Fueki, H. Tagawa, *Journal of Solid State Chemistry* **1989**, *80*, 102.
- [42] Y. Cao, M. J. Gadre, A. T. Ngo, S. B. Adler, D. D. Morgan, *Nat Commun* **2019**, *10*, 1346.
- [43] G. Cohn, E. D. Wachsman, *J. Electrochem. Soc.* **2017**, *164*, F3035.

[44] R. A. De Souza, *J. Mater. Chem. A* **2017**, *5*, 20334.

Figure Captions

Figure 1. Original isotopic exchange setup for experiments up to $P = 40$ bar and $T = 1,100$ °C.

Figure 2. Evolution of D^* coefficients measured at $pO_2 = 6.3$ bar as a function of temperature for the over-oxidized nickelates $La_2NiO_{4+\delta}$ (LNO, red circles), $Pr_2NiO_{4+\delta}$ (PNO, yellow squares) and $Nd_2NiO_{4+\delta}$ (NNO, orange triangles). The corresponding open black symbols along with the dashed lines (linear fit) give the D^* data for isotopic exchanges performed under $pO_2 = 0.2$ bar from the literature.

Figure 3. Evolution of D^* coefficients measured at $pO_2 = 6.3$ bar as a function of temperature for the oxide deficient perovskites $La_{0.6}Sr_{0.4}CoO_{3-\delta}$ (LSC, light blue circles) and $La_{0.6}Sr_{0.4}Fe_{0.8}Co_{0.2}O_{3-\delta}$ (LSCF, blue triangles) (Table 1). The corresponding open black symbols along with the dashed lines (linear fit) give the D^* data for isotopic exchanges performed under $pO_2 = 0.2$ bar from the literature.

Figure 4. Evolution of k^* coefficient measured at $pO_2 = 6.3$ bar as a function of temperature for the over-oxidized nickelates $La_2NiO_{4+\delta}$ (LNO, red circles), $Pr_2NiO_{4+\delta}$ (PNO, yellow squares) and $Nd_2NiO_{4+\delta}$ (NNO, orange triangles). The corresponding open black symbols along with the dashed lines (linear fit) give the k^* data for isotopic exchanges performed under $pO_2 = 0.2$ bar from the literature. The green symbols correspond to k^* for $La_2NiO_{4+\delta}$ measured for a shorter exchange time of 45 min.

Figure 5. Evolution of k^* coefficient measured at $pO_2 = 6.3$ bar as a function of temperature for the oxide deficient perovskites LSC (light blue circles) and LSCF (blue triangles). The corresponding open black symbols along with the dashed lines (linear fit) give the k^* data for isotopic exchanges performed under $pO_2 = 0.2$ bar from the literature. The green symbols correspond to k^* for LSC and LSCF, measured for a shorter exchange time of 2 h.

Figure 6. Evolution of δ with oxygen partial pressure at 700 °C in LSC materials.

Tables with Captions

Table 1. Oxygen over / under - stoichiometries delta (δ) values determined by TGA experiments performed under reducing atmosphere, on the samples before exchange (slowly cooled down to room temperature, RT) and on previously exchanged sample under ^{18}O atmosphere, quenched at a given temperature, under $p\text{O}_2 = 6.3$ bar.

Material		$\text{La}_2\text{NiO}_{4+\delta}$	$\text{Pr}_2\text{NiO}_{4+\delta}$	$\text{Nd}_2\text{NiO}_{4+\delta}$	$\text{La}_{0.58}\text{Sr}_{0.4}\text{CoO}_{3-\delta}$
Before exchange, at RT		0.16(2)	0.22(2)	0.21(3)	0.020(14)
Exchange temperature (T_{ex}) / °C	500	0.25(2)	0.31(2)	0.29(3)	0.010(14)
	550	-	0.33(2)	0.27(3)	-
	600	0.21(2)	0.43(2)	0.27(3)	0.010(14)
	650	-	0.36(2)	0.28(3)	-
	700	0.23(2)	0.50(2)	0.28(3)	0.003(10)



Figure 1:

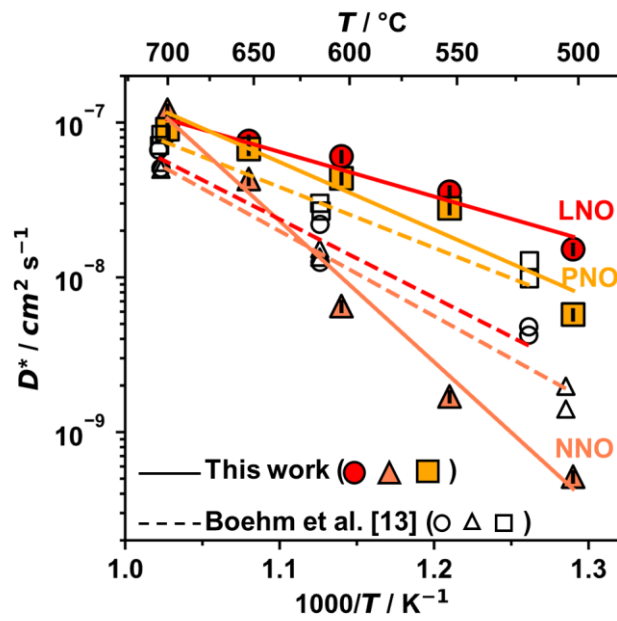


Figure 2:

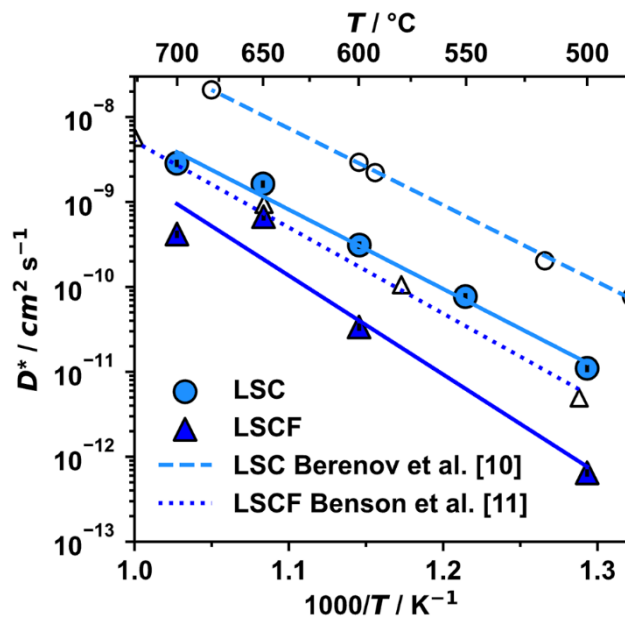


Figure 3:

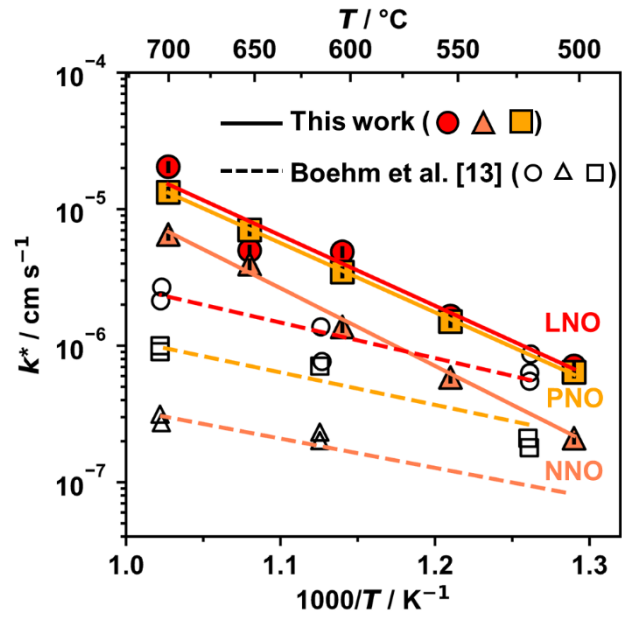


Figure 4:

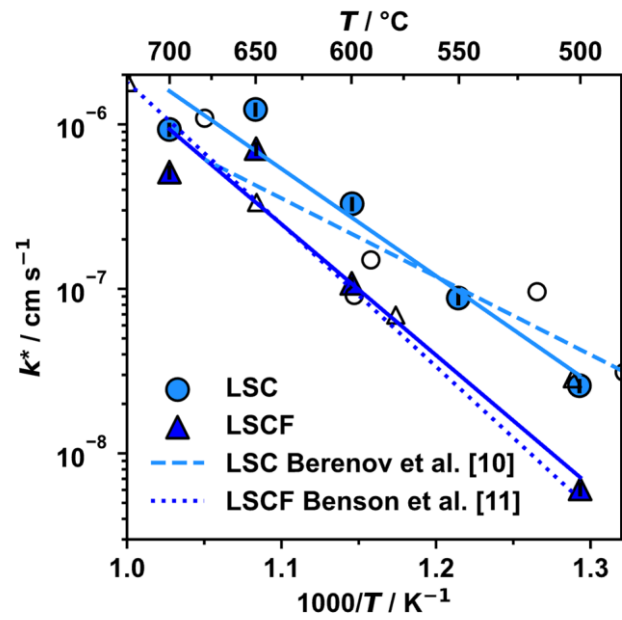


Figure 5:

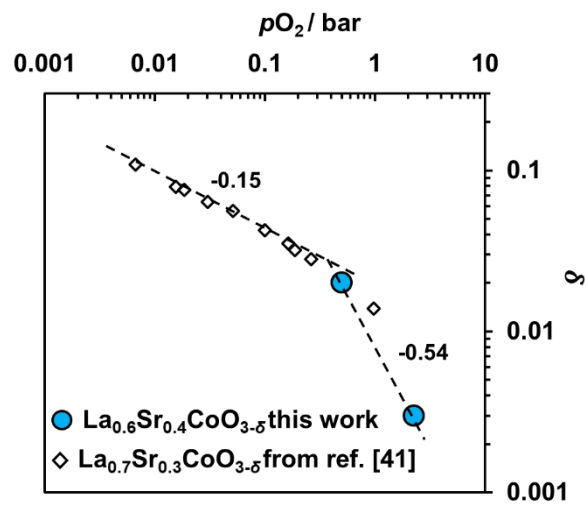


Figure 6: